Materials Advances

ROYAL SOCIETY OF CHEMISTRY

PAPER

View Article Online
View Journal | View Issue

Cite this: *Mater. Adv.*, 2025, 6, 5475

Impact of thermal treatment and magnetic field on the dynamic mechanical behavior of polyacrylonitrile nanofibers with embedded magnetic ferrite nanoparticles†

Baran Sarac,[ab] Viktor Soprunyuk,[c] Eray Yüce,[ad] Selin Gümrükçü,[e] Wilfried Schranz *[c] and A. Sezai Sarac[f]

Electrospun ferrite–polymer nanofiber composites exhibit an exclusive combination of electronic and material properties and tailorable functionalities. An incorporation of (cobalt) ferrite nanofillers to the polyacrylonitrile (PAN) matrix was corroborated by X-ray diffraction, where the systematic and organized arrangement of inorganic components was achieved through non-covalent bonding upon electrospinning, as proven by the energy dispersive X-ray attached to scanning electron microscopy. These nanomaterials exhibit the intrinsic electronic characteristics of the polymers due to the π-electron system of the C≡N group with oxide particles, as revealed by Fourier transmission infrared spectroscopy. By applying an external magnetic field during dynamic mechanical measurements under tension, expecially for the PAN/$CoFe_2O_4$, remarkable increase in the glass transition (~16 K) and activation energy (almost twice as high) along with a higher storage modulus are observed with the application of magnetic field in comparison to standard PAN nanofiber samples to be attributed to the magnetostrictive behavior of Co ferrite. The thermomechanical stability of the samples with undetectable weight loss was ascertained by thermogravimetric analysis. These results demonstrate that the nanofillers not only reinforce the polymer matrix but also introduce field-responsive mechanical characteristics, highlighting their potential in sensing, actuation, and smart material applications.

Received 10th April 2025,
Accepted 20th June 2025

DOI: 10.1039/d5ma00349k

rsc.li/materials-advances

1. Introduction

Ferrite is a ceramic compound containing iron oxide, known for its ferrimagnetic properties, making it attractive to magnets and magnetizable itself. It is typically hard, brittle, a poor electrical conductor, and resistant to high temperatures. Ferrites are cost-effective, have high resistivity, and are versatile, making them a valuable material in many industries.[1] Iron oxide nanoparticles (NPs) in small sizes exhibit superparamagnetic properties, where the magnetic moment of iron oxide nanoparticles can be improved, and the surface of ferrite nanoparticles can be modified by surfactants and polymers to increase their stability in solution.[2] Nanoferrites are extensively utilized as advanced oxides in biomedical applications, particularly for magnetic hyperthermia treatments, owing to their unique biocompatibility, persistent magnetic behavior and exceptional ability to generate localized heating for the destruction of tumor cells.[3] However, their use in cancer treatments demands specific characteristics, including biocompatibility, low toxicity, a high specific absorption rate (SAR), rapid attainment of the target hyperthermia temperature, nanoscale crystalline size compatible with biological systems, and minimal dosage requirements to achieve therapeutic efficacy.[4]

Among various ferrite materials, cobalt ferrite with the chemical composition of $CoFe_2O_4$ ($CoO{\cdot}Fe_2O_3$), stands out, where the material falls between soft and hard magnetic categories and is typically classified as semi-hard.[5] Its magnetostrictive properties can be adjusted by applying a magnetic uniaxial anisotropy, which is achieved by raising the crystal to an appropriate temperature and applying magnetization for several minutes by an external magnetic field.[6] The generated magnetic anisotropy in cobalt ferrite also provides advantages

[a] Austrian Academy of Sciences (ÖAW), Erich Schmid Institute of Materials Science, 8700 Leoben, Austria
[b] Chair of Casting Research, Montanuniversität Leoben, 8700 Leoben, Austria
[c] Faculty of Physics, Physics of Functional Materials, University of Vienna, 1090 Vienna, Austria. E-mail: wilfried.schranz@univie.ac.at
[d] Department of Materials Science, Chair of Materials Physics, Montanuniversität Leoben, 8700 Leoben, Austria
[e] Department of Chemistry, Istanbul Technical University, 34469 Istanbul, Turkey
[f] Polymer Science and Technology, Istanbul Technical University, 34469 Istanbul, Turkey

† Electronic supplementary information (ESI) available. See DOI: https://doi.org/10.1039/d5ma00349k

in enhancing the magnetoelectric effect in a composite.[7] Cobalt ferrite, a prominent member of the spinel ferrite family, exhibits an inverse spinel structure. In its ideal configuration, all Co^{2+} ions are located at the B sites, while Fe^{3+} ions are evenly distributed between the A and B sites. This material has garnered significant acclaim owing to its outstanding electromagnetic performance (*i.e.*, strong anisotropy, high coercivity, moderate saturation magnetization), exceptional chemical stability even at high temperatures, and mechanical hardness. These properties make cobalt ferrite an excellent candidate for applications in electronic parts, such as computer systems, recording devices, and magnetic cards.[8]

Fig. 1 illustrates the various applications of cobalt ferrites across different fields. Aside from its appealing magnetic properties, cobalt ferrite is a versatile material with applications in energy storage and conversion. It can serve as an electrocatalyst for the oxygen evolution reaction (OER) and is also used in the fabrication of electrodes for electrochemical capacitors (supercapacitors), enhancing their energy storage capabilities. For example, a simple electrospinning-based synthesis of $CoFe_2O_4$ spinel nanofibers exhibiting excellent electrocatalytic performance for both oxygen evolution and hydrogen peroxide reduction reactions.[9] Cobalt ferrite prepared with controlled morphology and size to enhance the surface area, and thus the number of active sites, has been published.[10] The evolution of their magnetic properties was systematically analyzed in terms of particle size and shape, emphasizing characteristics that optimize performance as permanent magnets. Notably, both saturation magnetization and remanent magnetization increase consistently with particle size, ultimately stabilizing at a constant value for sizes above 20 nm.[11] Cobalt ferrite particle (core)–polymer (shell) NPs can be incorporated into a polymer host matrix to generate mostly transparent polymer-based magneto-optic components.[12] A proof-of-concept all-optical magnetometer has been developed utilizing a nanocomposite material composed of a cobalt ferrite core encapsulated in a polymer shell. This magnetometer achieves a noise-equivalent magnetic field sensitivity of 50 nT $\sqrt{\text{Hz}^{-1}}$, demonstrating the potential of these highly transparent and magneto-optically responsive materials for applications in magnetic field sensing systems requiring high sensitivity. Traditional ferrite cores, often used in high-inductance coils and transformers, are brittle, rigid, and bulky, and their performance is heavily affected by external factors, *i.e.*, temperature, pressure, electromagnetic fields, and frequency. In contrast, Flexible printed circuits (FPCs) offer a more versatile alternative, capable of being processed into injection-molded parts or thin, flexible films. These materials can function at high temperatures (up to 200 °C) and are available in self-adhesive formats with thicknesses between 0.2 and 0.4 mm. FPCs are particularly effective in electromagnetic compatibility (EMC) applications, where they shield coils from metallic interference or absorb high-frequency disturbances above 500 MHz.[13]

In terms of biomedical uses, $CoFe_2O_4$ NPs can be utilized as an efficient magnetic resonance imaging contrast agent, which possesses higher magnetic susceptibility than iron oxide.[14] It can also be utilized as controlled and localized drug release, which is often coated with biocompatible polymers and targeting ligands.[15] In another study, the dressing's cellulose component was magnetized by developing magnetic cellulose through the grafting of $CoFe_2O_4$ NPs onto cellulose fibers using a layer-by-layer deposition method. This method effectively integrates magnetic functionality into the cellulose structure, offering potential applications in wound healing and temperature-responsive medical

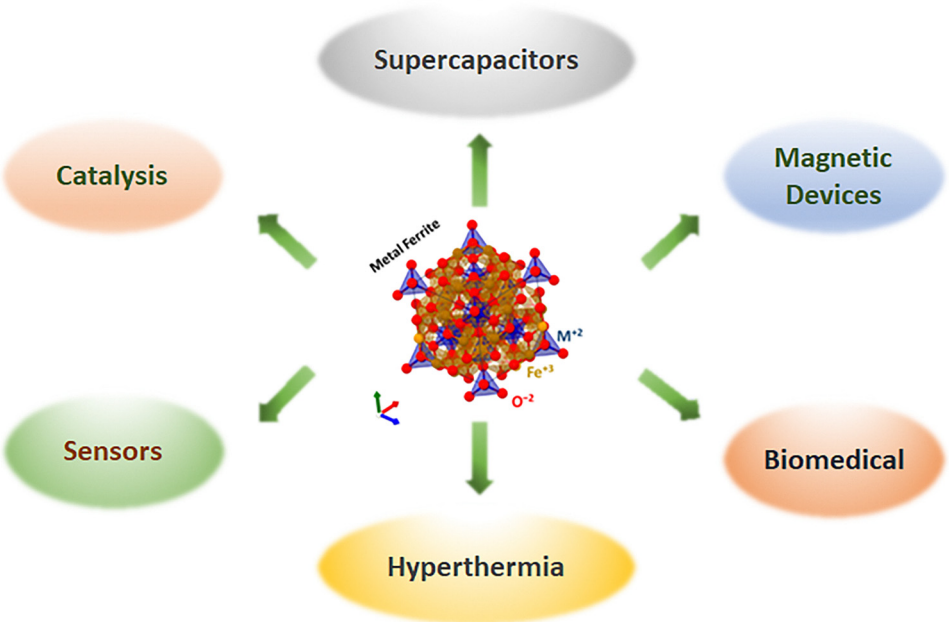

Fig. 1 Possible applications of magnetic cobalt ferrite ($CoFe_2O_4$) nanoparticles.

materials.[16] Cobalt ferrite NPs have a superior heating efficiency behavior with increased saturation magnetization when doped with other compounds. Also, it has a prominent measure of SAR parameters and thus makes a substantial pathway for hyperthermia treatments.[17]

Polyacrylonitrile (PAN), a widely recognized polymer known for its stability and mechanical properties. The properties of PAN are strongly influenced by its crystalline structures and the arrangement of its unit cells. However, the intrinsic properties of some PAN-based materials are often inadequate for specific applications. Nanoparticle fillers effectively modify the rheological behavior of PAN and its composite formulations, improving their processability. Moreover, when compared to microparticles of the same volume fraction, NPs significantly enhance the electrical, mechanical and chemical behavior of PAN, offering a more efficient solution for advanced material applications.[18]

The enhanced properties of PAN-based nanocomposite fibers, including those with carbon nanotubes, graphene, and inorganic NPs, are primarily attributed to the interfacial bonding between the nitrile groups in the polymer and the nanofillers. The enhanced properties of PAN nanofibers are linked to several factors, including the interfacial bonding of nitrile groups with nanofillers, their chemical composition, hydrophobicity, porosity, and wettability. Electrospun PAN nanofibers embedded with inorganic NPs, graphene nanosheets, graphene oxide, and carbon nanotubes are proposed for a broad range of advanced applications, such as supercapacitors, high-power batteries, filtration membranes, electromagnetic interference shielding, and strain sensors.[19,20] Surface-localized and homogenously dispersed magnetic particles on electrospun nanofibers offer significant advantages for sensing, actuation, and smart material applications due to their enhanced interfacial reactivity and stimulus responsiveness. For example, exposed ferrite or plasmonic NPs improve sensitivity and selectivity by facilitating direct interactions with target analytes, as demonstrated in gas sensors[21] and biosensors.[22] For actuation, magnetic NPs (*e.g.*, Fe_3O_4) on fiber surfaces enable rapid and precise deformation under external magnetic fields for actuators with programmable deformation.[23] In smart materials, stimuli-responsive particles such as thermoresponsive polymers[24] or metal oxide-containing hydrogel films[25] allow dynamic property modulation for adaptive textiles and drug delivery systems.[26]

Nanocomposite fibers composed of PAN incorporating carbon nanotubes (CNTs) and cobalt ferrite NPs were fabricated by electrospinning. Transmission electron microscopy reported the internal dispersion of the CNTs and $CoFe_2O_4$ NPs, and fibers exhibited electromagnetic interference shielding attenuation of about 3.9 dB.[27] Cobalt ferrite/PAN and cobalt ferrite/carbon nanofibers were synthesized through the electrospinning technique, and fiber magnetic properties measured by vibrating sample magnetometry indicate that $CoFe_2O_4$/PAN nanofibers have the saturation magnetization of 45 emu g^{-1}.[28] Incorporation of Fe-based nanofillers for the optimization of the polyacrylonitrile matrix was conducted to fabricate PAN nanofibers blended with iron oxide and MnZn Ferrite NPs through the introduction of an external magnetic field during dynamic mechanical measurements under tension.[29] For the PAN/MnZn Ferrite nanofibers, a relatively larger shift in T_g (10 K towards larger temperatures) is observed, emphasizing that, in comparison to Fe_2O_3, Mn^{2+} ions, in particular, enhance the material's magnetic response in MnZn Ferrite.

This paper presents a novel approach to synthesizing nearly monodisperse cobalt ferrite nanoparticles and their integration into polymer nanofibers, with a focus on their morphologic, spectroscopic, and thermodynamic properties. The superparamagnetic characteristics of cobalt ferrite NPs and their polymer-based nanocomposites are largely impacted by the particle size and distribution within the polymer matrix. The synthesis method for polymer nanocomposites doped with cobalt ferrite fillers, engineered as nanofibers, was detailed. We also compare their thermodynamic properties under varying magnetic fields to those of Fe_2O_3. Additionally, the morphological and spectroscopic attributes of the resulting materials are thoroughly investigated, highlighting the interplay between synthesis conditions and material performance. Distinct from prior studies focusing on other metal oxides, the novelty herein is the homogeneous dispersion of cobalt ferrite ($CoFe_2O_4$) nanoparticles within PAN nanofibers, which yields a quantifiable enhancement in thermal stability through an elevated glass transition temperature and a significant increase in stiffness around T_x, linked to the relatively less interaction of NPs with CN groups of PAN with minimum oxide surrounding NPs.

2. Materials and methods

2.1. Material

Polyacrylonitrile (PAN, molecular weight average of 150 000, CAS No.: 25014-41-9) and *N*,*N*′-dimethylformamide (DMF, purity $\geq$99.8%, CAS No.: 68-12-2) were procured from Sigma Aldrich. Iron oxide nanopowder (γ-Fe_2O_3, purity 99.9%, average particle diameter 10 nm, laser synthesized, near-spherical morphology, CAS No.: 1309-37-1) and cobalt ferrite nanoparticles ($CoFe_2O_4$, purity 99.9%, average particle diameter 30 nm, synthesized by chemical reagants, spherical morphology, CAS No.: 12052-28-7) were sourced by US Research Nanomaterials, Inc. All reagents used were of analytical grade and were employed without additional purification.

2.2. Preparation of PAN/metal oxide nanoparticle composite fibers

The electrospinning device consists of a syringe pump, a grounded aluminum collector, and a high-voltage DC power supply capable of delivering positive voltages up to 50 kV. The syringe pump allowed precise control of the polymer solution feed rate, adjustable between 5.5 μL h^{-1} and 20 mL h^{-1}. A syringe fitted with a needle (outer diameter: 0.7 mm) connected to a positive electrode was used to eject the polymer solution. Electrospinning was performed horizontally under ambient conditions, with an applied voltage ranging between

10 and 15 kV. The polymer solutions were ejected at a constant feed rate of 1 mL h^{-1}, and the separation between the collector and needle tip was kept at approximately 15 cm to ensure consistent nanofiber formation. Co ferrite microparticles (5 wt%) were mixed with 10 mL of 10% PAN solution in a cup horn sonicator *via* stirring overnight, which enables the PAN/$CoFe_2O_4$ to be dissolved in a dimethyl formamide solution. Nanofibers were successfully produced through continuous electrospinning for 3 hours, with no evidence of sedimentation in the polymer nanofiller solution throughout the process. Following each electrospinning trial, no visible sedimentation was detected within the syringe, indicating stable dispersion of the nanofillers in the solution.

2.3. Characterization methods

Dynamic mechanical analysis (DMA) was performed using a PerkinElmer DMA-8000 instrument over a temperature range of 300–800 K at a controlled 5 K min^{-1} heating rate. Measurements were performed in tension mode under sinusoidal forces at frequencies of 0.5, 5, and 15 Hz. Test specimens were fabricated in sheet geometry with dimensions approximately 10 mm × 7.5 mm × 0.13 mm to suit the tension testing configuration. Thermogravimetric analysis (TGA, TA Instruments) was performed by heating scans from room temperature to 800 °C at a rate of 20 °C min^{-1} under inert nitrogen atmosphere. X-ray diffraction (XRD) was conducted in Bragg–Brentano (θ–2θ) geometry by means of a Bruker D2 Phaser diffractometer equipped with a LYNXEYE-2 detector. Measurements were carried out over an angular range of 5° to 100°, utilizing Co Kα radiation (wavelength, λ = 0.17902 nm) with a step size of 0.005°. Data smoothing was performed using the Savitzky–Golay filter with a 20-point window and a second-order polynomial to enhance the signal quality. Imaging was performed using a TESCAN MAGNA scanning electron microscope (SEM), which offers ultra-high resolution and high-contrast capabilities. To enhance conductivity and achieve a high signal-to-noise ratio, the samples were sputtered with a 1–2 nm layer of graphite *via* sputtering. Magnifications ranging from 500× to 100 000× were employed. SEM imaging was conducted at an acceleration voltage of 20 keV, a beam current of 1 nA, an aperture size of 30 μm, and a working distance of ~12.5 mm. The same device was used at 20 kV acceleration voltage for the subsequent energy dispersive X-ray (EDX) mapping on the same samples using Quanta FEG 250 with an attached EDX detector. The information was processed using the software AZtec (OXFORD INSTRUMENTS). Average diameter and standard deviation of the nanofibers were measured from 50 single nanofibers through ImageJ Software. Attenuated total reflectance Fourier-transform infrared (ATR-FTIR) spectroscopy was implemented through a Bruker Vertex 70 ATR spectrometer covering the wavenumber range of 600–4000 cm^{-1}. The room temperature magnetic properties were assessed by alternating gradient field magnetometer (AGFM) within a ±10 kOe magnetic field range.

3. Results and discussion

3.1. Morphological and compositional characterization

The homogenous distribution of the nanofibers was ensured by low-magnification SEM imaging (Fig. 2a). White round-looking spots corresponding to the $CoFe_2O_4$ agglomerates were observed and accounted for the minimization of the high surface energy of the NPs within the PAN matrix.[29] The PAN matrix encapsulates these particle agglomerates, leading to round-looking morphologies.[30] The magnified imaging displays that particles (shown by the red arrows) join nanofibers (Fig. 2b) as well as are embedded within the nanofibers upon electrospinning (Fig. 2c). The average size of the PAN/$CoFe_2O_4$ nanofibers measured from the SEM images is 310 ± 40 nm. This value is much smaller than pure PAN (970 ± 110 nm) and PAN/Fe_2O_3 (520 ± 50 nm) nanofibers. Visible surface roughness is observed for all sample types, which can be attributed to the inherent nature of the electrospinning process, where the rapid solidification of polymer jets leads to the formation of irregular

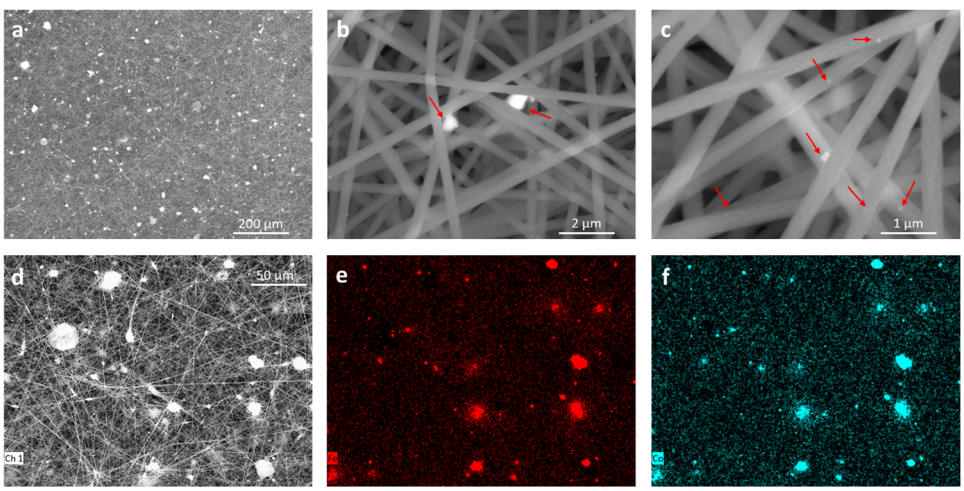

Fig. 2 Scanning electron microscopy of PAN/$CoFe_2O_4$ electrospun nanofilms at (a) 500×, (b) 50k× and (c) 100k×. (d) 2k× imaging and the corresponding EDX for (e) Fe and (f) Co elements.

fiber deposition and topographical variations. The compositional analysis of a representative region (Fig. 2d) identifies the existence of Fe (Fig. 2e) and Co (Fig. 2f) dispersed throughout the nanofibers as well as within the agglomerated regions. The SEM imaging of the PAN/Fe_2O_3 nanofibers shows a similar nanoparticle dispersion (Fig. S1a, ESI†). The EDX imaging (Fig. S1b, ESI†) and the corresponding qualitative elemental analysis confirm that the bright particles correspond to Fe_2O_3 NPs (Fig. S1c and d, ESI†).

3.2. Structural characterization

X-ray diffraction can reveal the type of crystalline within an semi-crystalline PAN polymer. Fig. 3a presents a comparative XRD analysis of the PAN, PAN/$CoFe_2O_4$ and PAN/Fe_2O_3 samples over the 5° and 100° 2θ range. The diffuse peaks at ~19.5° correspond to the orthorhombic PAN (110) reflection.[31] This peak shifts towards larger values, *i.e.*, ~19.8°, with the inclusion of NPs, indicating that the average unit lattice becomes smaller. The broad and less intense peak between 23–33° corresponds to the (002) reflection of PAN.[32] As confirmed formerly by the nanopowder diffraction analysis of Fe_2O_3 and PAN/Fe_2O_3 composite,[29] the peaks at ~35.5°, ~41.8°, ~51.0°, ~67.7°, and ~74.8° corresponds to (220), (311), (400), (511) and (440) reflections of the nanopowders, respectively (Fig. 3b). For the PAN/$CoFe_2O_4$ nanofiber, compared to PAN/Fe_2O_3, there is a slight shift of the peak towards larger angles, *i.e.*, ~0.3° shift of the (311) peak.

3.3. FTIR-ATR spectroscopic analysis

Fig. 4a shows the FTIR-ATR comparison of the PAN/$CoFe_2O_4$, PAN/Fe_2O_3 and PAN reference samples. The significant broadening of the peak at ~3620 cm^{-1} may suggest interactions between the hydroxyl groups on the ferrite phase and the cyanoethyl groups (–C≡N triple bond) of PAN. Additionally, the spectra exhibited a wide absorption band between 3100–3600 cm^{-1}, which validates the interaction between the nitrile groups and Co^{2+} ions.[33] The peak observed around 2920 cm^{-1} and a shoulder peak at ~2860 cm^{-1} accounts for the stretching vibrations of the –C–H bonds within the CH_2 groups of the PAN structure.[34] The FTIR spectrum of PAN reveals characteristic peaks at 2240 cm^{-1}, associated with the stretching vibrations of the –C≡N triple bond, indicating potential interactions between ferrite and polyacrylonitrile. The peak intensity decreases when $Co_2Fe_2O_4$ is added instead of Fe_2O_3, referring to the high interaction of this type of blend. PAN is polymerized in the presence of cobalt(II) salts. The peaks detected at approximately 1660 cm^{-1} and 1450 cm^{-1} are characteristic of pristine PAN nanofibers, corresponding to the –C=O group in the amide structure and the –C≡N stretching vibrations, respectively.[35] C–H bending and CH_2 wagging are recorded at 1360 cm^{-1}, C–H wagging is at 1256 cm^{-1}, and C–C stretching of PAN polymer chain at 1070 cm^{-1}, and CH_2 rocking at 777 cm^{-1}.[36] The band at 538 cm^{-1} is linked to the oscillation of Fe–O bonds.[37]

New peaks are detected at 1540 and 1577 cm^{-1} for the $Co_2Fe_2O_4$ interaction with the PAN compared to PAN itself and PAN/Fe_2O_3 nanofibers, clearly indicating above mentioned interaction of CN group, especially with cobalt (Fig. 4b). Table 1 indicates the comparison of the FTIR peaks 1450 cm^{-1} to 2920 cm^{-1} and 1662 cm^{-1} to 2920 cm^{-1}. The areal ratio of absorbances of FTIR peaks (FTIR (A_2/A_1) C≡N/C–H) decreases in the order of PAN/$CoFe_2O_4$ < PAN/Fe_2O_3 < PAN owing to the varying extent of interaction of NPs with CN groups of PAN.

C–H functionalization/activation reactions within a range of polymers using Fe_2O_3 or MFe_2O_4 (M: metal) containing oxide NPs were reported.[38] The Fe–O bonds in the NPs can participate in hydrogen bonding with the C–H bonds next to the cyanide (C≡N) bonds in PAN (see Fig. 6), where such non-covalent bonds are interactions between molecules or atoms that do not involve sharing electrons. Their importance lies in their ability to form weak yet specific interactions between molecules, which are crucial for many functions in living systems and materials. This type of interaction can contribute to forming a network between the NPs and PAN, decreasing the fiber dimensions and quenching their strength and elasticity.

3.4. Dynamic mechanical analysis

DMA results indicate the differences between the pure PAN sample at 0 mT and PAN/$CoFe_2O_4$ samples at 0, 40 and 100 mT

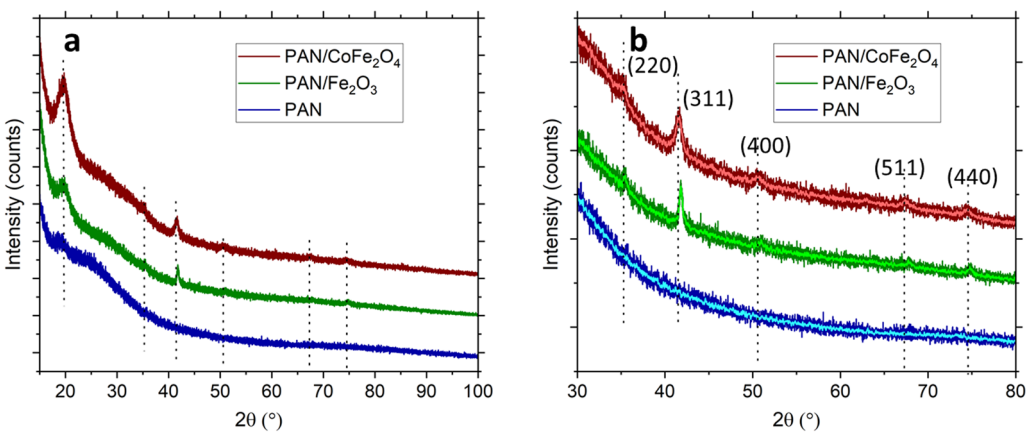

Fig. 3 (a) Full XRD spectra of the PAN/$CoFe_2O_4$, PAN/Fe_2O_3 and PAN samples. (b) Close-up region with smoothed curves to indicate the peak positions.

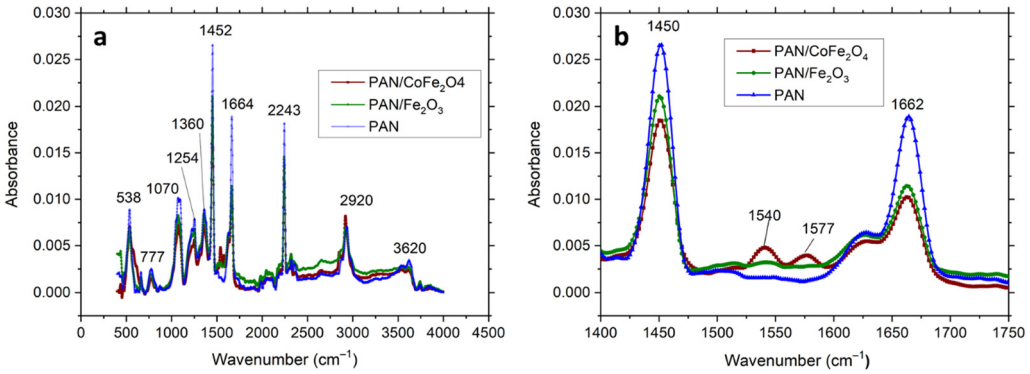

Fig. 4 (a) FTIR spectra of the $CoFe_2O_4$ and Fe_2O_3 containing PAN as well as pure PAN sample in the range of 400–4000 cm^{-1}. (b) Close-up region displaying the range 1400–1750 cm^{-1}.

Table 1 Comparison of peak areal ratios for the FTIR spectroscopy normalized to the highest peak

Type	FTIR (A_2/A_1) (1450 cm^{-1})/ (2920 cm^{-1})	FTIR (A_2/A_1) 1662 cm^{-1}/ 2920 cm^{-1}	C≡N/C–H
$PAN/CoFe_2O_4$	2.27	1.22	3.25/2.27 = 1.43 (A_2 for 1450 cm^{-1})
PAN/Fe_2O_3	2.91	1.64	2.65/1.22 = 2.16 (A_2 for 1662 cm^{-1})
PAN	3.25	2.65	

externally applied field under 0.5 Hz (Fig. 5a). Even though no remarkable difference between the glass transition T_g points is observed for the PAN and $PAN/CoFe_2O_4$ samples at 0 mT, a large T_g shift by ~15 K towards larger temperatures is observed by the application of an external magnetic field. The largest change is observed for the crystallization temperature T_x (from ~587 K); there is a gradual rise in the storage modulus Y' for the pure PAN sample, whereas a very steep rise from 50 MPa to 750 MPa was observed for the $PAN/CoFe_2O_4$ sample. The enhanced storage modulus observed in metal oxide-PAN fibers at high temperatures compared to pure PAN fibers is a result of the integration of metal oxide NPs. These NPs act as reinforcing agents, remarkably enhancing the mechanical properties of the composite material until 750 K, and the key factors contributing to this enhancement. Strong interfacial bonding facilitates the effective transfer of load from the polymer matrix to the NPs, thereby enhancing the overall stiffness of the composite.

Metal oxides can also enhance the thermomechanical stability of the PAN fibers. This increased thermal resistance can help sustain the mechanical attributes of the composite at higher temperatures (in the studied range) in comparison to the absence of metal oxide in PAN nanofiber, in contrast to our previous TGA data of PAN polymer and PAN NF under an inert (nitrogen) atmosphere.[39] The steepness of this rise attenuates to 350 MPa by the application of a 40 mT external field, but with a clear shift in T_x to 610 K. An early rupture of the sample below T_x was recorded for the $PAN/CoFe_2O_4$ sample under a 120 mT external field. The largest losses in modulus Y'' are observed at T_g and T_x for the $PAN/CoFe_2O_4$ sample without the application of an external field, which is pronouncedly lower for the pure PAN sample. Compared to PAN/Fe_2O_3 at 0 mT reaching 800 K, the PAN/Fe_2O_3 under 120 mT is broken at 665 K before reaching the maximum Y'' value. A clear comparison of the PAN (Fig. 5b) and $PAN/CoFe_2O_4$ (Fig. 5c) samples for three different frequencies of 0.5, 5 and 15 Hz was drawn. The activation energy E_a of each sample found from the T_g measurements at frequencies of 0.5, 5 and 15 Hz show distinct differences (Fig. 5d). A remarkable increase in E_a for the $PAN/CoFe_2O_4$ sample with the influence of magnetic field (from 299 ± 38 to 573 ± 62 kJ mol^{-1}) was recorded, meaning that the field can cause particle rearrangement or stiffening, restricting molecular motion and increasing E_a. This is also understood by the sharp stiffening observed for the magnetic nanoparticle containing PAN samples after T_x, except for the virgin PAN sample. The influence of homogenously dispersing only 5 wt% of ferrite-based NPs within PAN was also reflected in reaching full magnetic saturation with a well-defined sigmoidal shape, indicating a smooth magnetization reversal.[40,41]

Fig. S2 (ESI†) shows the thermogravimetric analysis (TGA) of the electrospun PAN nanofibers produced in this study. The crystallization peak is at 561 K, where the crystallization leads to a weight loss of ~37%. The second small peak at 704 K is related to the onset of degradation, as also confirmed by the onset of decrease in storage modulus in Fig. 5, with a further weight loss of ~24%. The weight loss persists until the end of the measurement (1073 K), where compared to the initial state, a total weight loss of ~70% was recorded.

In the former study, it was shown that PAN/MnZn Ferrite nanofibers show a more pronounced shift in T_g and T_x compared to PAN/Fe_2O_3, linked to the complex spinel structure of MnZn Ferrites with enhanced response to external magnetic field. $PAN/CoFe_2O_4$ shows a very similar increase in T_g (~15 K) but with an earlier rupture with an applied magnetic field (120 mT). On the contrary, the molecular motions of PAN chains are more hindered or constrained in the presence of $CoFe_2O_4$ NPs than with MnZn ferrite (MnZn–Fe_2O_4), evidenced by the higher stiffness after exceeding the T_x when no external field was applied.[29]

Along with the homogenous particle dispersion, finer nanofibers typically provide a higher surface area-to-volume ratio,

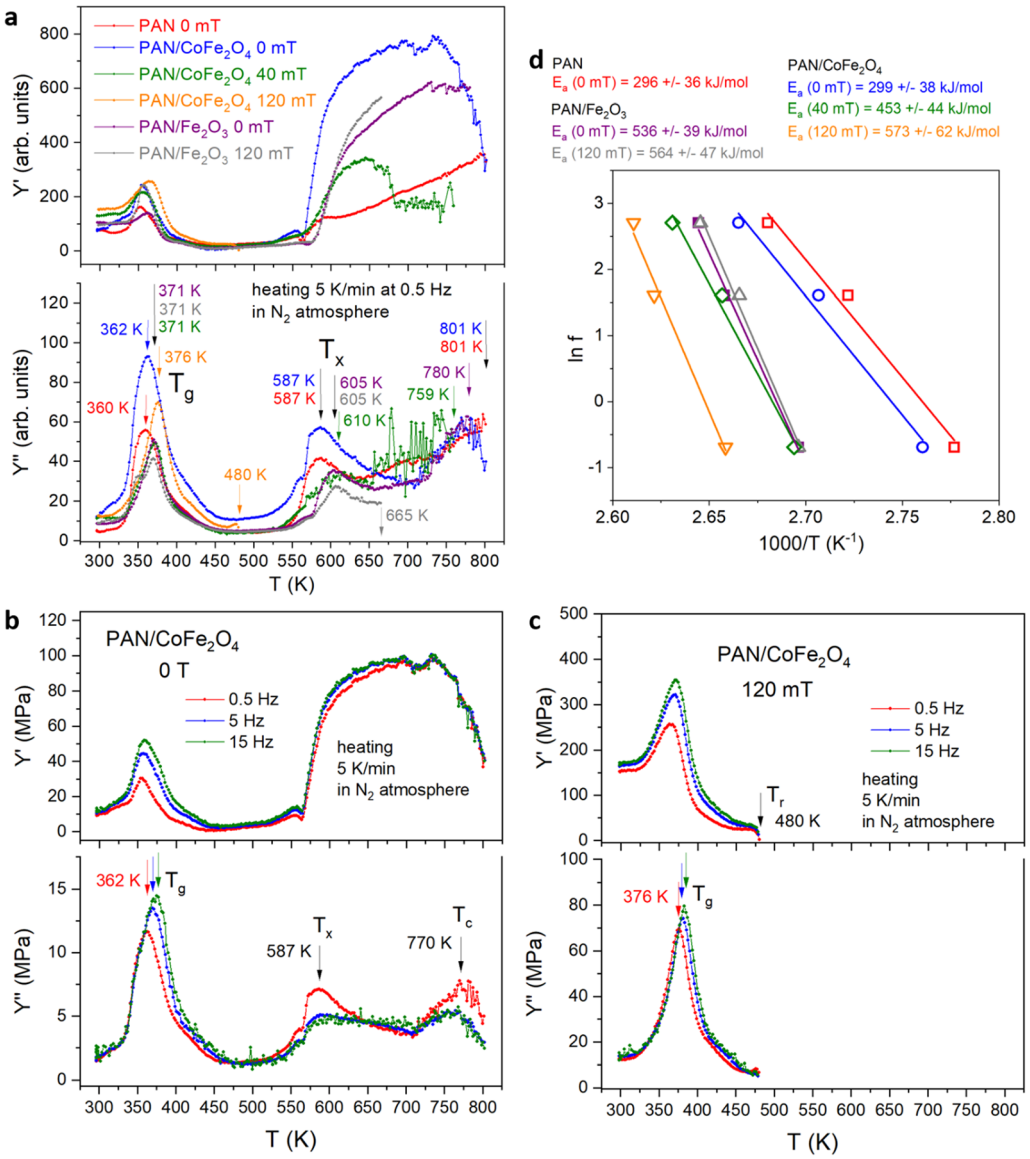

Fig. 5 (a) Dynamic mechanical analysis comparison of the investigated PAN, PAN/Fe_2O_3 and PAN/$CoFe_2O_4$ (for 0 T, 40 mT and 120 mT) at 5 K min^{-1} heating rate between 300 K and 800 K. Frequency dependence of PAN/$CoFe_2O_4$ at (b) 0 T and (c) 120 mT. (d) Activation energies for the PAN, PAN/Fe_2O_3 and PAN/$CoFe_2O_4$ samples at various magnetic fields.

leading to increased interfacial interactions within the matrix, which can enhance stiffness. Additionally, as also observed here, smaller fiber diameters restrict polymer chain mobility more effectively, which can lead to higher storage modulus and a shift in the glass transition temperature (T_g) toward higher values. Conversely, larger or irregularly distributed nanofibers may introduce defects or weak interfaces, reducing mechanical reinforcement and thermomechanical stability.[42,43]

3.5. Magnetic property analysis

Alternative gradient field magnetometer (AGFM) shows a gradual and smooth magnetization with a complete magnetic saturation at 10 kOe. Table 2 depicts the magnetic property comparison of PAN/Fe_2O_3 and PAN/$CoFe_2O_4$. PAN/$CoFe_2O_4$ shows a lower saturation magnetization (M_s) and higher coercivity (H_c) accounted for by the stronger magnetocrystalline anisotropy.[44] In polymer composites, saturation magnetization (M_s) decreases for both $CoFe_2O_4$ and Fe_2O_3 due to magnetic dilution and spin disorder, while coercivity (H_c) generally decreases as well, though $CoFe_2O_4$ tends to retain higher Hc than Fe_2O_3 probably due to its intrinsic anisotropy.

3.6. Possible interaction of ferrite nanoparticles with PAN

Ferrites can interact with PAN and undergo redox reactions with the C≡N group of PAN at possibly high temperatures. The C≡N groups in the polymer might act as reducing agents, reducing Fe_2O_3 to a lower oxidation state (*i.e.*, FeO or Fe).[45] Within composite metal oxide layers, the interaction of molecules containing the C≡N group involves two primary mechanisms. Firstly, the π-electron system of the C≡N group

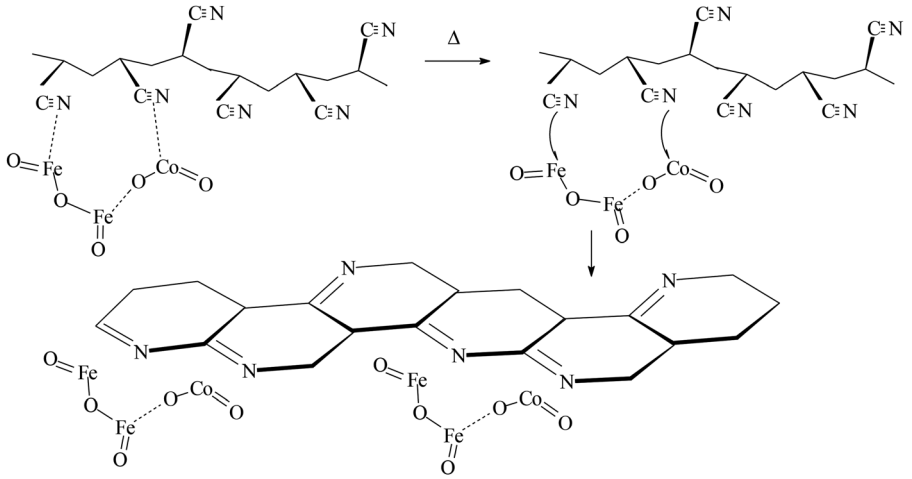

Fig. 6 Possible interaction between Co Ferrite with PAN during thermomechanical treatment.

Table 2 Magnetic properties of PAN/Fe_2O_3 *vs.* PAN/$CoFe_2O_4$

	M_s (emu g^{-1})	M_r (emu g^{-1})	H_c (Oe)
PAN/Fe_2O_3	6.4	1.1	106
PAN/$CoFe_2O_4$	4.7	1.4	369

can interact with the π-electron systems present in metal oxide clusters,[46] such as nanoparticles or nanowires. This interaction is favored by the electron-rich nature of the triple bond in the C≡N group, and these molecules can participate in redox reactions with species that have acquired electrons from the surrounding polymer matrix (Fig. 6). The mechanism of electron ''capture'' from the polymer matrix can vary and may involve processes like charge transfer complexes or electron transfer reactions. The specific characteristics of these interactions, including the type of metal oxide, the size and morphology of the clusters, and the properties of the polymer matrix, considerably impact the overall behavior of the composite material.

Stabilization (cyclization) of PAN during thermomechanical treatment in the presence of Fe_2O_3 NPs in PAN Nanofiber matrix was reported previously by our group.[29] Furthermore, the nanocatalytic behavior of iron nanoparticles is reported for reduction reactions.[47] A key step during this process was the association structures generated by the interaction of hydrogen bonds under heat treatment and the cyclization structures composed of C=N bonds. The heat treatment process for PAN based carbon fibers critically relies on a chemical transformation known as the cyclization reaction, *i.e.*, the cyclization reaction of PAN/Fe_2O_3 nanofiber (and for the PAN/Co Ferrite nanofibers as well), is promoted by the catalytic effect of Fe_2O_3 recorded during thermomechanical measurements.

4. Conclusion

The incorporation of metal oxide nanoparticles into PAN nanofibers significantly enhances their high-temperature properties, making them suitable for various advanced applications. These composite fibers exhibit improved thermomechanical stability, mechanical reinforcement in composites, and enhanced insulation properties due to the interaction between metal oxides and the C≡N groups in PAN ascertained by FTIR spectroscopy. The redox interactions between ferrites and PAN facilitate structural modifications, including cyclization, which is catalyzed by (cobalt) ferrites during thermomechanical processing.

Characterization techniques such as HRSEM, XRD, spectroscopy, and thermomechanical analysis confirm the well-dispersed nanoparticle distribution and strong interfacial interactions within the polymer matrix. Compared to Fe_2O_3, the globally and homogeneously dispersed Co-ferrite NPs ensured by XRD and SEM-EDX imaging demonstrate superior thermomechanical stability by shifting the glass transition temperature towards higher values, thereby improving the overall thermal performance of the nanocomposite.

Furthermore, PAN/$CoFe_2O_4$ NFs exhibit promising electrochemical properties, making them viable for energy storage applications, including supercapacitors and oxygen evolution reaction (OER) electrocatalysis. Optimizing the morphology and surface area of cobalt ferrite NPs can further enhance their electrochemical activity by increasing the density of active sites.

These findings underline the multifunctional potential of PAN/$CoFe_2O_4$ nanofibers, which makes them strong candidates for integration into next-generation energy storage systems, flexible electronic devices, and high-temperature composite materials. Future work should focus on tailoring the NP architecture—through size control, doping strategies, or template-assisted synthesis—to further improve performance. Additionally, scaling up fabrication methods and assessing long-term operational stability will be essential steps toward translating these materials into practical, industrial applications.

Conflicts of interest

There are no conflicts to declare.

Data availability

The data supporting this article have been included as part of the ESI.†

Acknowledgements

This article is based upon work from COST Action NanoSpace CA21126 and COST Action COSY CA21101, supported by COST (European Cooperation in Science and Technology).

References

1 R. C. Pullar, Hexagonal ferrites: A review of the synthesis, properties and applications of hexaferrite ceramics, *Prog. Mater. Sci.*, 2012, **57**, 1191–1334, DOI: **10.1016/j.pmatsci.2012.04.001**.

2 M. Mahdavi, M. B. Ahmad, M. J. Haron, F. Namvar, B. Nadi, M. Z. A. Rahman and J. Amin, Synthesis, Surface Modification and Characterisation of Biocompatible Magnetic Iron Oxide Nanoparticles for Biomedical Applications, *Molecules*, 2013, **18**, 7533–7548, DOI: **10.3390/molecules18077533**.

3 S. Laurent, D. Forge, M. Port, A. Roch, C. Robic, L. Vander Elst and R. N. Muller, Magnetic Iron Oxide Nanoparticles: Synthesis, Stabilization, Vectorization, Physicochemical Characterizations, and Biological Applications, *Chem. Rev.*, 2008, **108**, 2064–2110, DOI: **10.1021/cr068445e**.

4 G. Nandhini and M. K. Shobana, Role of ferrite nanoparticles in hyperthermia applications, *J. Magn. Magn. Mater.*, 2022, **552**, 169236, DOI: **10.1016/j.jmmm.2022.169236**.

5 S. J. Salih and W. M. Mahmood, Review on magnetic spinel ferrite (MFe_2O_4) nanoparticles: From synthesis to application, *Heliyon*, 2023, **9**, e16601, DOI: **10.1016/j.heliyon.2023.e16601**.

6 J. C. Slonczewski, Origin of Magnetic Anisotropy in Cobalt-Substituted Magnetite, *Phys. Rev.*, 1958, **110**, 1341–1348, DOI: **10.1103/PhysRev.110.1341**.

7 A. Aubert, V. Loyau, F. Mazaleyrat and M. LoBue, Enhancement of the Magnetoelectric Effect in Multiferroic $CoFe_2O_4$/PZT Bilayer by Induced Uniaxial Magnetic Anisotropy, *IEEE Trans. Magn.*, 2017, **53**, 1–5, DOI: **10.1109/TMAG.2017.2696162**.

8 M. Mylarappa, V. Venkata Lakshmi, K. R. Vishnu Mahesh, N. Raghavendra and H. P. Nagaswarupa, Cyclic Voltammetry, Impedance and Thermal Properties of $CoFe_2O_4$ Obtained from Waste Li-Ion Batteries, *Mater. Today: Proc.*, 2018, **5**, 22425–22432, DOI: **10.1016/j.matpr.2018.06.612**.

9 M. Li, Y. Xiong, X. Liu, X. Bo, Y. Zhang, C. Han and L. Guo, Facile synthesis of electrospun MFe_2O_4 (M = Co, Ni, Cu, Mn) spinel nanofibers with excellent electrocatalytic properties for oxygen evolution and hydrogen peroxide reduction, *Nanoscale*, 2015, **7**, 8920–8930, DOI: **10.1039/C4NR07243J**.

10 J.-L. Ortiz-Quiñonez, S. Das and U. Pal, Catalytic and pseudocapacitive energy storage performance of metal (Co, Ni, Cu and Mn) ferrite nanostructures and nanocomposites, *Prog. Mater. Sci.*, 2022, **130**, 100995, DOI: **10.1016/j.pmatsci.2022.100995**.

11 A. López-Ortega, E. Lottini, C. d J. Fernández and C. Sangregorio, Exploring the Magnetic Properties of Cobalt-Ferrite Nanoparticles for the Development of a Rare-Earth-Free Permanent Magnet, *Chem. Mater.*, 2015, **27**, 4048–4056, DOI: **10.1021/acs.chemmater.5b01034**.

12 A. Lopez-Santiago, H. R. Grant, P. Gangopadhyay, R. Voorakaranam, R. A. Norwood and N. Peyghambarian, Cobalt ferrite nanoparticles polymer composites based all-optical magnetometer, *Opt. Mater. Express*, 2012, **2**, 978–986, DOI: **10.1364/OME.2.000978**.

13 Ferrites and accessories-Ferrite polymer composites General information, EPCOS AG - TDK Group Company, 05/2017, **https://www.tdk-electronics.tdk.com/download/531550/c467ba21dc521448ad776058e6c01e86/pdf-ferritepolymer.pdf**.

14 Z. Mohammadi, N. Attaran, A. Sazgarnia, S. A. M. Shaegh and A. Montazerabadi, Superparamagnetic cobalt ferrite nanoparticles as T_2 contrast agent in MRI: in vitro study, *IET Nanobiotechnol.*, 2020, **14**, 396–404, DOI: **10.1049/iet-nbt.2019.0210**.

15 F. Javed, M. A. Abbas, M. I. Asad, N. Ahmed, N. Naseer, H. Saleem, A. Errachid, N. Lebaz, A. Elaissari and N. M. Ahmad, Gd^{3+} Doped $CoFe_2O_4$ Nanoparticles for Targeted Drug Delivery and Magnetic Resonance Imaging, *Magnetochemistry*, 2021, **7**, 47, DOI: **10.3390/magnetochemistry7040047**.

16 S. Williams, C. L. Okolie, J. Deshmukh, L. Hawco, J. McNeil, A. C. Nganou Assonkeng, C. Bennett and M. Mkandawire, Magnetizing Cellulose Fibers with $CoFe_2O_4$ Nanoparticles for Smart Wound Dressing for Healing Monitoring Capability, *ACS Appl. Bio. Mater.*, 2019, **2**, 5653–5662, DOI: **10.1021/acsabm.9b00731**.

17 A. J. Giustini, A. A. Petryk, S. M. Cassim, J. A. Tate, I. Baker and P. J. Hoopes, Magnetic Nanoparticle Hyperthermia In Cancer Treatment, *Nano Life*, 2010, **1**, 1–23, DOI: **10.1142/s1793984410000067**.

18 T. A. Adegbola, O. Agboola and O. S. I. Fayomi, Review of polyacrylonitrile blends and application in manufacturing technology: recycling and environmental impact, *Res. Eng.*, 2020, **7**, 100144, DOI: **10.1016/j.rineng.2020.100144**.

19 A. Kausar, Polyacrylonitrile-based nanocomposite fibers: A review of current developments, *J. Plast. Film Sheeting*, 2019, **35**, 295–316, DOI: **10.1177/8756087919828151**.

20 M. Aslam, T. Khan, M. Basit, R. Masood and Z. A. Raza, Polyacrylonitrile-based electrospun nanofibers—A critical review, *Materialwiss. Werkstofftech.*, 2022, **53**, 1575–1591, DOI: **10.1002/mawe.202200150**.

21 P. M. Bulemo, D.-H. Kim, H. Shin, H.-J. Cho, W.-T. Koo, S.-J. Choi, C. Park, J. Ahn, A. T. Güntner, R. M. Penner and I.-D. Kim, Selectivity in Chemiresistive Gas Sensors: Strategies and Challenges, *Chem. Rev.*, 2025, **125**, 4111–4183, DOI: **10.1021/acs.chemrev.4c00592**.

22 J. Zhou, J. Zheng, C. Wang, G. Zhang, H. Yang, F. Xiong, M. Fan, Z. Wang, Y. Li and C. Yang, Electrospun biosensors for biomarker detection, *Colloid Interface Sci. Commun.*, 2024, **59**, 100767, DOI: **10.1016/j.colcom.2024.100767**.

23 Y. Zhai, C. Gong, J. Chen and C. Chang, Magnetic-field induced asymmetric hydrogel fibers for tough actuators with programmable deformation, *Chem. Eng. J.*, 2023, **477**, 147088, DOI: **10.1016/j.cej.2023.147088**.

24 L. Deng, J. Chen, Z. Zhang and W. Zeng, Thermo-responsive PNIPAm-based Composite Nanofibers Prepared by Electrospinning, *Int. J. Electrochem. Sci.*, 2018, **13**, 7347–7355, DOI: **10.20964/2018.08.63**.

25 N. Sudhakaran, M. Abraham, P. A. Parvathy, S. Das and S. K. Sahoo, Flexible and thermoresponsive AEMR-pNIPAM/$Cs_{0.33}WO_3$ composite hydrogel film with NIR shielding potential for smart windows and smart curtains, *Chem. Eng. J.*, 2024, **490**, 151603, DOI: **10.1016/j.cej.2024.151603**.

26 R. Ziegler, S. Ilyas, S. Mathur, G. F. Goya and J. A. Fuentes-García, Remote-Controlled Activation of the Release through Drug-Loaded Magnetic Electrospun Fibers, *Fibers*, 2024, **12**, 48, DOI: **10.3390/fib12060048**.

27 X. Jin, Q.-Q. Ni, Y. Fu, L. Zhang and T. Natsuki, Electrospun nanocomposite polyacrylonitrile fibers containing carbon nanotubes and cobalt ferrite, *Polym. Compos.*, 2012, **33**, 317–323, DOI: **10.1002/pc.21251**.

28 I. H. Chen, C.-C. Wang and C.-Y. Chen, Fabrication and characterization of magnetic cobalt ferrite/polyacrylonitrile and cobalt ferrite/carbon nanofibers by electrospinning, *Carbon*, 2010, **48**, 604–611, DOI: **10.1016/j.carbon.2009.09.062**.

29 B. Sarac, V. Soprunyuk, G. Herwig, S. Gümrükçü, E. Kaplan, E. Yüce, W. Schranz, J. Eckert, L. F. Boesel and A. S. Sarac, Thermomechanical properties of confined magnetic nanoparticles in electrospun polyacrylonitrile nanofiber matrix exposed to a magnetic environment: structure, morphology, and stabilization (cyclization), *Nanoscale Adv.*, 2024, **6**, 6184–6195, DOI: **10.1039/d4na00631c**.

30 D.-H. Wang, J. Su, Y.-M. Liu, Y. Yu, Y. Su, G.-X. Xie, L.-L. Jiang, L.-N. Zhou, D.-Y. Zhu, S.-H. Chen, J.-S. Yan, X.-X. Wang and Y.-Z. Long, Recent advances in electrospun magnetic nanofibers and their applications, *J. Mater. Chem. C*, 2022, **10**, 4072–4095, DOI: **10.1039/D2TC00107A**.

31 F. Kayaci, S. Vempati, C. Ozgit-Akgun, N. Biyikli and T. Uyar, Enhanced photocatalytic activity of homoassembled ZnO nanostructures on electrospun polymeric nanofibers: A combination of atomic layer deposition and hydrothermal growth, *Appl. Catal., B*, 2014, **156–157**, 173–183, DOI: **10.1016/j.apcatb.2014.03.004**.

32 Z. Zhang, L. Zhang, S. Wang, W. Chen and Y. Lei, A convenient route to polyacrylonitrile/silver nanoparticle composite by simultaneous polymerization–reduction approach, *Polymer*, 2001, **42**, 8315–8318, DOI: **10.1016/S0032-3861(01)00285-3**.

33 R. Syrlybaeva, N. Movsum-zade, I. Safiullina, Y. Puzin and E. Movsum-zade, Polymer-metal complexes of polyacrylonitrile and its copolymers: synthesis and theoretical study, *J. Polym. Res.*, 2015, **22**, 100, DOI: **10.1007/s10965-015-0716-4**.

34 E. V. Loginova, I. V. Mikheev, D. S. Volkov and M. A. Proskurnin, Quantification of copolymer composition (methyl acrylate and itaconic acid) in polyacrylonitrile carbon-fiber precursors by FTIR-spectroscopy, *Anal. Methods*, 2016, **8**, 371–380, DOI: **10.1039/C5AY02264A**.

35 Q. Liu, N. Xu, L. Fan, A. Ding and Q. Dong, Polyacrylonitrile (PAN)/TiO_2 mixed matrix membrane synthesis by thermally induced self-crosslinking for thermal and organic-solvent resistant filtration, *Chem. Eng. Sci.*, 2020, **228**, 115993, DOI: **10.1016/j.ces.2020.115993**.

36 E. Cipriani, M. Zanetti, P. Bracco, V. Brunella, M. P. Luda and L. Costa, Crosslinking and carbonization processes in PAN films and nanofibers, *Polym. Degrad. Stab.*, 2016, **123**, 178–188, DOI: **10.1016/j.polymdegradstab.2015.11.008**.

37 H. T. Vu, M. B. Nguyen, T. M. Vu, G. H. Le, T. T. T. Pham, T. D. Nguyen and T. A. Vu, Synthesis and Application of Novel Nano Fe-BTC/GO Composites as Highly Efficient Photocatalysts in the Dye Degradation, *Top. Catal.*, 2020, **63**, 1046–1055, DOI: **10.1007/s11244-020-01289-w**.

38 S. Dutta, P. Kumar, S. Yadav, R. D. Sharma, P. Shivaprasad, K. S. Vimaleswaran, A. Srivastava and R. K. Sharma, Accelerating innovations in CH activation/functionalization through intricately designed magnetic nanomaterials: From genesis to applicability in liquid/regio/photo catalysis, *Catal. Commun.*, 2023, **175**, 106615, DOI: **10.1016/j.catcom.2023.106615**.

39 I. Gergin, E. Ismar and A. S. Sarac, Oxidative stabilization of polyacrylonitrile nanofibers and carbon nanofibers containing graphene oxide (GO): a spectroscopic and electrochemical study, *Beilstein J. Nanotechnol.*, 2017, **8**, 1616–1628, DOI: **10.3762/bjnano.8.161**.

40 F. Alahmari, F. A. Khan, H. Sozeri, M. Sertkol and M. Jaremko, Electrospun Cu-Co ferrite nanofibers: synthesis, structure, optical and magnetic properties, and anti-cancer activity, *RSC Adv.*, 2024, **14**, 7540–7550, DOI: **10.1039/d3ra08087k**.

41 B. Sarac, E. Sharifikolouei, M. Micusik, A. Scalia, Z. Najmi, A. Cochis, L. Rimondini, G. Barrera, M. Coisson, S. Gümrükcü, E. Yüce and A. S. Sarac, Ferrite-based polyacrylonitrile composite nanofiber membranes as implantable local mesenchymal cell growth, *Emergent Mater.*, 2025, DOI: **10.48550/arXiv.2506.22527**.

42 Z. M. Huang, Y. Z. Zhang, M. Kotaki and S. Ramakrishna, A review on polymer nanofibers by electrospinning and their applications in nanocomposites, *Compos. Sci. Technol.*, 2003, **63**, 2223–2253, DOI: **10.1016/S0266-3538(03)00178-7**.

43 D. Li and Y. Xia, Electrospinning of Nanofibers: Reinventing the Wheel, *Adv. Mater.*, 2004, **16**, 1151–1170, DOI: **10.1002/adma.200400719**.

44 E. A. Gorbachev, E. S. Kozlyakova, L. A. Trusov, A. E. Sleptsova, M. A. Zykin and P. E. Kazin, Design of modern magnetic materials with giant coercivity, *Russ. Chem. Rev.*, 2021, **90**, 1287, DOI: **10.1070/RCR4989**.

45 H. P. DeGroot and T. P. Hanusa, Cyanide Complexes of the Transition Metals, in *Encyclopedia of Inorganic and Bioinorganic Chemistry*, John Wiley & Sons, Ltd, 2020, DOI: **10.1002/9781119951438.eibc0055.pub2**.

46 L. I. Trakhtenberg, M. I. Ikim, O. J. Ilegbusi, V. F. Gromov and G. N. Gerasimov, Effect of Nanoparticle Interaction on Structural, Conducting and Sensing Properties of Mixed

Metal Oxides, *Chemosensors*, 2023, **11**, 320, DOI: **10.3390/chemosensors11060320**.

47 Z. He, H. Liu, S. Zhang, J. Yang, C. Jiang, M. Ji, J. Yu, M. Wang, C. Zhu and J. Xu, Investigation of the Cyclization Mechanism of Poly(acrylonitrile-*co*-ethylenesulfonic acid) Copolymer during Thermal Oxidative Stabilization by In Situ Infrared Spectroscopy, *Ind. Eng. Chem. Res.*, 2020, **59**, 9519–9531, DOI: **10.1021/acs.iecr.0c00977**.